Int. J. Electron. Commun. (AEÜ) 194 (2025) 155749

Contents lists available at ScienceDirect

Int. J. Electron. Commun. (AEÜ)

journal homepage: www.elsevier.com/locate/aeue

Regular paper

Wideband omnidirectional radiation linearly polarized antenna for UHF and DTV applications

Shokooh Sadat Kooshki [a], Fatemeh Dehghani [a], Keivan Kaboutari [b,c], Javad Ghalibafan [a,*]

[a] Department of Electrical Engineering, Shahrood University of Technology, Shahrood, Iran
[b] Instituto de Telecomunicações and Department of Electronics, Telecommunications and Informatics, University of Aveiro, 3810-193 Aveiro, Portugal
[c] Department of Mechanical Engineering, Carnegie Mellon University, Pittsburgh, PA 15213, United States of America

ARTICLE INFO

Keywords:
UHF omnidirectional antenna
Linear radiation polarization
Wideband
DTV applications

ABSTRACT

An innovative wideband omnidirectional linearly polarized antenna is presented in this paper that is specially designed for Ultra-High Frequency (UHF) applications, with a particular focus on Digital Television (DTV) broadcasting. The proposed antenna operates across a frequency range of 479–808 MHz, ensuring sufficient coverage for DTV applications. Key design features include the use of four-paired crossed-dipole antennas, encircling parasitic elements, and concentric circular circles on an FR4 substrate to enhance impedance bandwidth and gain. The fabricated antenna demonstrates a measured reflection coefficient better than -15 dB over the critical 550–750 MHz frequency band, achieving a peak gain of 0.90–1.35 dBi with stable performance across its operational spectrum. Its omnidirectional radiation pattern, characterized by a 360° E-plane and 121.2° H-plane Half Power Beam Width (HPBW), makes it ideal for uniform signal coverage in DTV broadcasting. The design prioritizes compactness with dimensions of $0.56\lambda \times 0.56\lambda \times 0.005\lambda$, meeting space constraints for practical deployment. Detailed simulations and experimental validation demonstrate the antenna's effectiveness in achieving its design objectives. This work advances wideband UHF antenna technology, offering a reliable and cost-effective solution for industrial broadcasting applications. The proposed design is optimized for manufacturability, ensuring compatibility with high-volume production.

1. Introduction

Ultra High Frequency (UHF) antennas are essential components of modern wireless communications systems [1]. UHF antennas operate within the frequency range of 0.3–3 GHz (International Telecommunication Union (ITU) standard)/0.3–1 GHz (Institute of Electrical and Electronics Engineers (IEEE) standard), and they are essential in a number of industries, including broadcasting, telecommunications, and navigation. The UHF antenna spectrum is mainly divided into 0.3–0.4 GHz, 0.4–0.7 GHz, 0.7–1 GHz and 1–3 GHz sub-bands with applications in air traffic control and military communications [2], public safety communications and terrestrial Television (TV) broadcasting, mobile telecommunications (including Long Term Evolution (LTE) and 5G) [3–5] and Digital Television (DTV) broadcasting [6,7], and Internet of Things (IoT) devices, Global Positioning System (GPS), and satellite communications [2,8], respectively. Several types of wireless services benefit from UHF's ability to balance propagation characteristics, such as moderate penetration through obstacles and high data transmission rates [9]. Depending on the application, optimized gain, directional or omnidirectional patterns, and linear or circular polarization characteristics of UHF antennas should be considered before final design and fabrication. Indeed, these parameters guarantee signal strength and ensure efficient power delivery over desired coverage areas with trade-offs in range and coverage uniformity. As a result, the design specifications and performance characteristics of these devices are critical to ensuring efficient signal transmission and reception in a wide range of environments. Nevertheless, sub-bands of the UHF frequency band spectrum may also be used for other applications that should be avoided from interfering with each other.

An antenna with a share-aperture feed is designed in [2] for satellite applications in the UHF/S frequency bands. The antenna is constructed in a stacked configuration with a UHF element on the lower layer and a 4 × 4 array of S-band elements on the upper layer. Both bands' critical features are circular polarization, low mutual coupling, and high port isolation, with frequency ranges of 300–400 MHz for UHF and 1.9–2.3 GHz for S-band. The study in [6] presents a horizontally polarized omnidirectional antenna for DTV reception in the UHF band (470–862 MHz) using stacked curved dipoles. However, the measured

* Corresponding author.
E-mail address: jghalibafan@shahroodut.ac.ir (J. Ghalibafan).

https://doi.org/10.1016/j.aeue.2025.155749
Received 27 December 2024; Accepted 28 February 2025
Available online 10 March 2025
1434-8411/

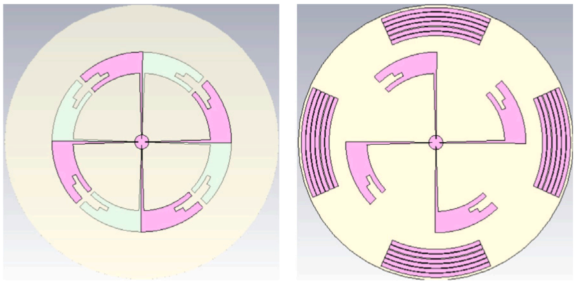

(a) four-paired crossed-dipole antennas (front- and back-side).

(b) The addition of encircling parasitic elements on the front-side.

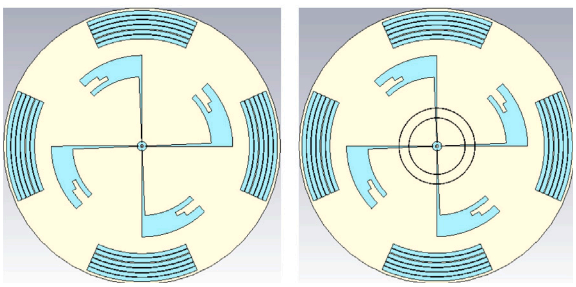

(c) The addition of encircling parasitic elements on the back-side.

(d) The addition of paired concentric circles on the back-side.

Fig. 1. An outline of the proposed structure's design flow.

gain ranges between −10 dBi and 0.67 dBi, which is relatively low and may limit the effectiveness of the antenna in weak signal areas. Furthermore, the measured cross-polarization levels were higher than those simulated, particularly in the elevation plane (up to −9 dB), which could affect performance in certain environments.

In [7], a broadband printed dipole antenna design with an integrated balun and a tuning element for DTV applications is proposed. The authors have proposed a tuning mechanism that allows the frequency range of the antenna to be adjusted to closely cover the specified DTV band. Considering the measured data, it covers an impedance bandwidth of 414.5 MHz from 457.7 to 872.2 MHz, which covers the frequency band of DTV systems (470–862 MHz). In addition, the proposed antenna has a horizontally polarized omnidirectional radiation pattern with a maximum realized gain of 2.95 dBi. According to the paper, a broadband circularly polarized conformal antenna for spaceborne applications is presented [8]. In this design, the antenna operates at frequencies of 390–450 MHz. It features an air microstrip cross-slot structure conformally mounted to the satellite surface. As a result of its innovative design, it is capable of achieving a peak gain of 6.7 dBic, an axial ratio bandwidth of 27.2% and an impedance bandwidth of 32.5%. Its compact and lightweight design, circular polarization and broadband performance make it an ideal choice for satellite and missile communications systems requiring reliable wide-angle coverage and long range.

Research presented in [10] describes an optically transparent dual-band antenna for UHF and S-band applications fabricated from Indium Tin Oxide-coated Polyethylene Terephthalate (ITO-PET) and soda lime glass (SLG) substrate. As a dual-band antenna, it operates between 1.6 and 2 GHz and 3.25 and 4.95 GHz and utilizes a slotted circular structure with a modified ground plane to improve performance. Although ITO-PET has relatively low conductivity, the antenna has a positive gain, reasonable radiation efficiency (43.51–45.13%), and sufficient bandwidth to meet consumer electronic applications demands.

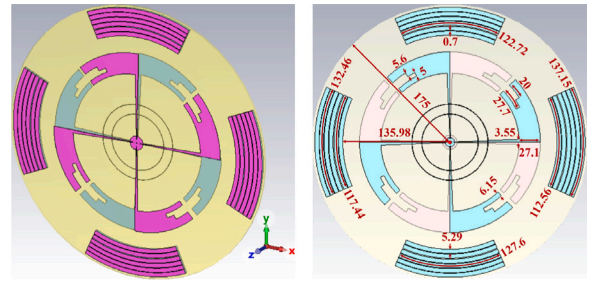

(a) 3D view (front- and back-side).

(b) Front- and back-side view.

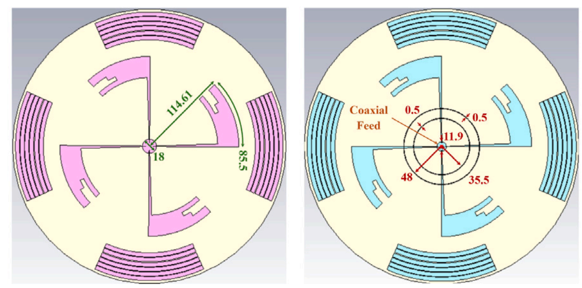

(c) Front-side view.

(d) Back-side view.

Fig. 2. Structure of the proposed antenna. Dimensions are given in millimeters.

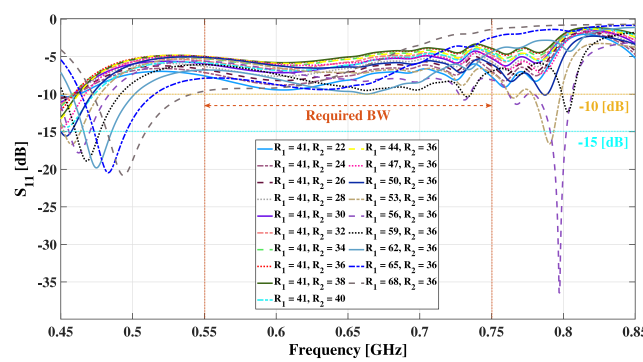

Fig. 3. Simulated S_{11} when the concentric circles' outer (R_1) and inner (R_2) radii on both sides of the proposed antenna sweep using the same amount.

The material's transparency (>83%) makes it suitable for integration into contemporary designs, such as smart windows and wearable electronics, without compromising visual accessibility. A horizontally polarized omnidirectional antenna loaded with Cylindrical Ring Dielectric (CRD) for wideband applications in the 2G/3G/LTE communication bands is described in [11]. In this antenna, an Alford-structure Loop Antenna (ASLA) is combined with a CRD, significantly improve the impedance and radiation pattern bandwidth. A wide operating bandwidth of 1.63–2.8 GHz (52.8%) is achieved by the proposed structure. Despite its compact size of $0.55\lambda \times 0.55\lambda \times 0.057\lambda$, the antenna achieves a maximum gain of 1.56 dBi at 1.66 GHz with ≤1.4 dB gain variation in the horizontal plane.

An omnidirectional wideband horizontally polarized antenna is presented in [12] for use in 2G/3G/LTE networks. The antenna incorporates four driven cross-shaped slots and four parasitic cross-shaped slots arranged symmetrically on a circular substrate to achieve wideband operation with compact dimensions of $0.53\lambda \times 0.53\lambda \times 0.005\lambda$ (where λ is the free-space wavelength at the lowest frequency). Operating within a frequency range of 1.62 to 2.81 GHz (53.7%), it achieves a gain of 0.9 to 1.3 dBi with a stable response. The parasitic slots increase the impedance bandwidth and reduce the gain variation across the azimuth plane to less than 1.7 dB. Modern wireless system signals are efficiently covered by the antenna's omnidirectional radiation pattern and low cross-polarization level of 27 dB. According to [13], a horizontally polarized omnidirectional antenna using stacked curved dipoles has been proposed for DTV reception. This antenna is made of thin brass sheets and operates in the UHF band (470–862 MHz). It provides horizontal polarization and an omnidirectional radiation pattern. The structure consists of stacked dipoles separated by an air gap and fed by a 75 Ω coaxial transmission line. The optimized design provides impedance matching ($|S_{11}| \le 10$ dB) and covers a bandwidth of 467 MHz (404–871 MHz). It provides a gain of −10 to 0.67 dBi with a low cross-polarization of −15 dB in measurements. The incorporation of branching curves significantly improves the operational bandwidth and impedance characteristics. With a compact and lightweight design, the antenna is suitable for mobile stations, vehicles and other applications requiring robust DTV signal reception over large areas.

An antenna in [14] combines a cylindrical Dielectric Resonator Antenna (DRA) and an Alford loop to achieve orthogonal electric fields with equal amplitude and 90° phase difference, enabling omnidirectional CP radiation. The final prototype demonstrated impedance bandwidths of 35 MHz, 185 MHz, and 135 MHz, with axial ratio bandwidths of 70 MHz, 120 MHz, and 28 MHz, respectively. The antenna exhibited omnidirectional CP patterns and average gains of 1.2 dBic, 1.6 dBic, and −1.5 dBic across the bands. In [15], a reconfigurable antenna based on an Alford loop and a circular array of tunable electric-LC (ELC) resonators is presented. The antenna operates from 2.0 to 2.4 GHz (18.2% bandwidth) and achieves beam steering with an 18° angular resolution in the azimuth plane. Enhanced by a 3D-printed dielectric lens and Vivaldi-shaped slots, it achieves a realized gain of 6.2–8.2 dBi and a Front-to-Back Ratio (FBR) of 13–23 dB, making it suitable for applications requiring omnidirectional or directional radiation with horizontal polarization. An omnidirectional antenna for 2.4/5 GHz Wi-Fi applications is demonstrated in [16]. In this design, an Electrically Small (ES) loop is incorporated for the lower band and an Alford for the upper band on a single substrate, resulting in a compact diameter of $0.296\lambda_0$. The antenna exhibits low gain variation (<1 dB) in the azimuthal plane and high efficiency (~90%).

This study proposes a UHF Alford loop antenna for DTV broadcasting applications with linear radiation polarization. As a matter of fact, this antenna was designed for DTV applications aboard ships where only linear and horizontal polarizations with omnidirectional patterns are needed due to the loss of signals received by linear and vertical polarizations. It should be noted that traditional UHF antennas often face challenges in achieving a balance between wide bandwidth, stable gain, and omnidirectional radiation patterns, which are crucial for uniform signal coverage in broadcasting applications. However, the novelty of this design lies in its innovative use of double concentric circular structures on an FR4 substrate. This feature enhances the antenna's impedance bandwidth and gain without introducing other parasitic or complex structures, allowing it to operate effectively across the 479–808 MHz frequency range.

The antenna is designed based on simulation results and optimized for maximum gain. This design has been tested and evaluated for performance and has been found to be suitable for TV broadcasting applications. In accordance with the company's requirements, the intended antenna must cover the 480–800 MHz frequency range (bandwidth (BW)), while ensuring its S_{11} parameter is less than −15 dB in the 550–750 MHz frequency spectrum. Additionally, the proposed antenna must have a positive and preferably greater than 0.75 dBi peak gain; while meeting restrictions aligned with the dimensions, i.e., it must be compact in size. In this proposal, the antenna has a peak gain of 0.90–1.35 dBi and dimensions of $0.56\lambda \times 0.56\lambda \times 0.005\lambda$, much smaller than the restrictions (λ is the wavelength at the beginning of the BW). The antenna exhibits a stable gain in its BW with oscillations less than 0.215 dBi.

2. Design methodology of the proposed antenna

The proposed antenna was designed using the full-wave CST Studio Suite simulator for DTV applications covering the frequency band of 479–808 MHz. Initially, a planar four-paired crossed-dipole antennas employing the Coaxial Probe Feed (CPF) excitation method was designed based on an FR4 substrate with 4.4 relative permittivity and 0.025 loss tangent to maximize production efficiency and minimize production costs. As a first step, four-paired crossed-dipole antennas are designed and optimized, Fig. 1(a). However, parasitic elements (Figs. 1(b) and 1(c)) and concentric circles (Fig. 1(d)) are added to the structure to fully touch the company's requirements regarding the BW and peak gain of the required antenna. Based on simulation results for bare planar four-paired crossed-dipole antennas, it was found that the bandwidth of the antennas was limited and covered a narrow frequency spectrum with low peak gain. Therefore, the antenna bandwidth can be increased as well as the peak gain by adding parasitic elements on both sides of the antenna configuration. As a result of the parasitic elements, the radiation pattern was confined at the radiation direction, thereby increasing the peak gain of the proposed structure. Parasitic strips also significantly suppress antenna reactance and improve return loss. An important point to note is that parasitic elements were selected and adjusted based on simulation results in order to increase the bandwidth and peak gain of the designed antenna. In conclusion, by incorporating a pair of concentric circles into the antenna design, better impedance matching across the BW was achieved, improving the antenna's performance over the desired frequency range. Basically, the multi-stage structure adjustment was generally intended to further increase peak gain and bandwidth by confining the radiation pattern and improving the antenna's impedance matching.

Indeed, the proposed configuration includes four-paired crossed-dipole antennas with encircling parasitic elements on both sides of the structure, as well as two concentric circles on the rear side, Fig. 2. Then, it was optimized using a parametric study procedure to obtain satisfactory performance. A millimeter scale is provided over the figure to indicate the dimensions of the proposed structure. The designed antenna has dimensions of $0.56\lambda \times 0.56\lambda \times 0.005\lambda$, much smaller than the restrictions for antenna compactness (λ is the wavelength at the beginning of the BW). Fig. 2 illustrates the proposed antenna structure from different perspectives.

As mentioned, the authors were forced to use planner structures due to dimension restrictions. Then, as an initial step, four-paired crossed-dipole antennas are designed and optimized to cover the 480–800 MHz frequency band with DTV applications. Furthermore, the proposed antenna's return loss is enhanced by the use of encircling parasitic elements on both sides of the structure. Nevertheless, the optimized structure's return loss and BW did not meet the company's requirements, Fig. 9. It is worth noting that the final simulated and measured reflection coefficient for the proposed antenna should have been better than −15 dB in the 550–750 MHz frequency band. However, the criteria for reflection coefficient and BW were not met.

Based on simulation studies, the authors determined that concentric circles may enhance BW and increase return loss depth. As a means of improving the BW and return loss of the proposed structure and fulfilling the prerequisites, two outer and inner concentric circles with R_1 and R_2 radii are located on both sides of the antenna (totally four concentric circles), and parametric studies are conducted. Throughout this study, the radii of the concentric circles, R_1 and R_2, vary equally and simultaneously on both sides of the structure. Based on the simulation results presented in Fig. 3, it can be concluded that this approach will not produce estimated results.

Next, the effect of the same concentric circles on both sides of the structure is evaluated when the circles' radii are swept independently. R_1 and R_4 are the outer radii of the concentric circles on the back- and front-side of the structure. In the same way, R_2 and R_3 are the inner radii of the concentric circles on the back- and front-side of the

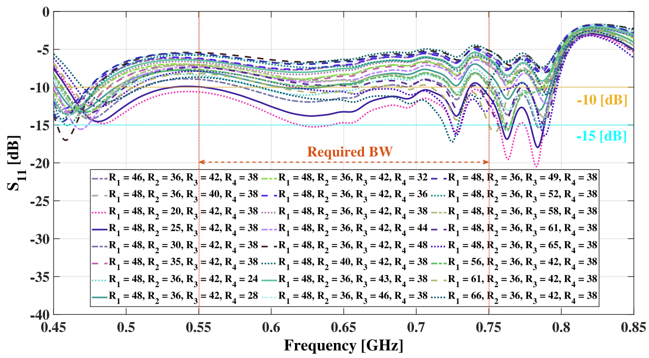

Fig. 4. Simulated S_{11} when the outer (R_1 (back-side circle) & R_4 (front-side circle)) and inner (R_2 (back-side circle) & R_3 (front-side circle)) radii of the concentric circles on both sides of the proposed antenna sweep independently.

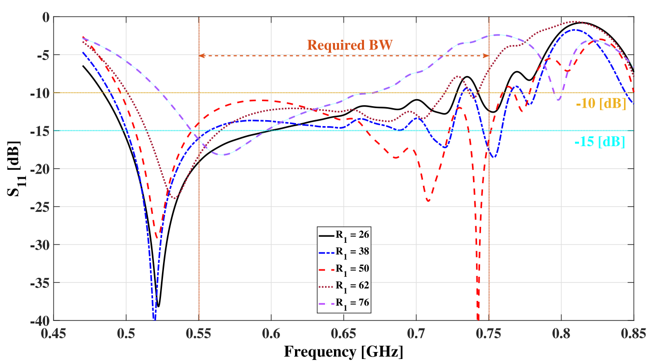

Fig. 5. Simulated S_{11} when the radius of the concentric circle (R_1) on the back-side of the proposed antenna sweeps.

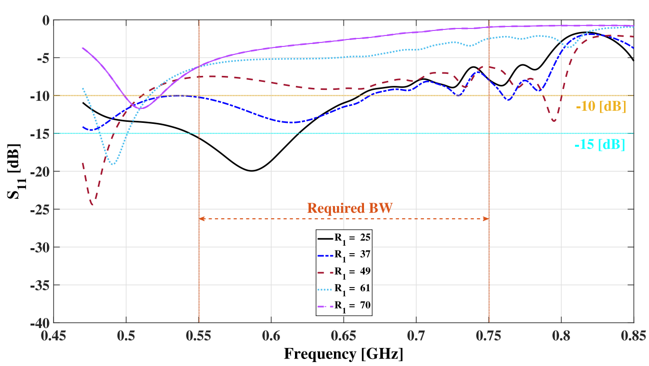

Fig. 6. Simulated S_{11} when the concentric circles' radii (R_1) on both sides of the proposed antenna sweep using the same amount.

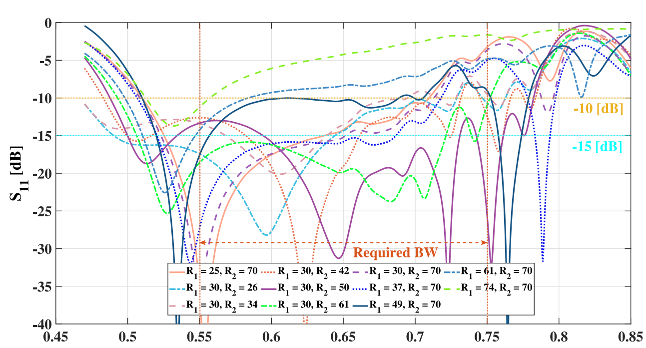

Fig. 7. Simulated S_{11} when the back-side with R_1 and front-side with R_2 radii of the concentric circles on both sides of the proposed antenna sweep independently.

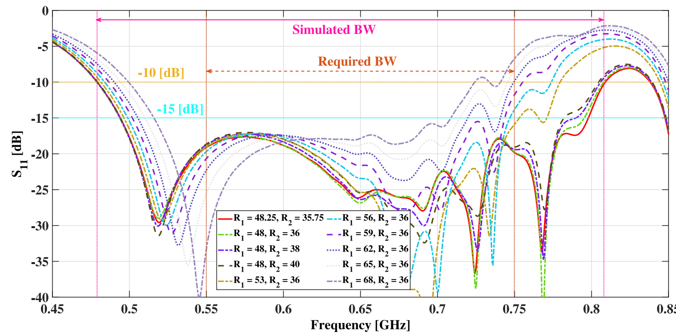

Fig. 8. Simulated S_{11} when the outer (R_1) and inner (R_2) radii of the concentric circles on the back-side of the proposed antenna sweep independently.

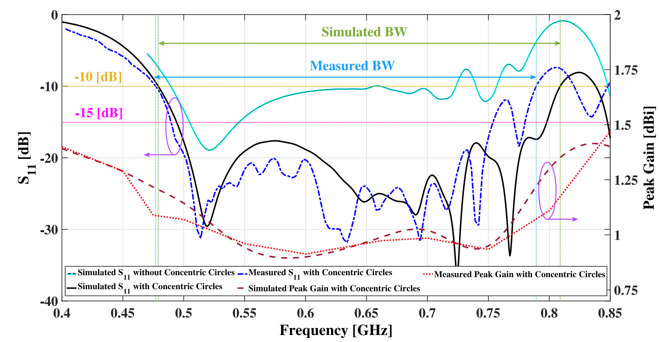

Fig. 9. Simulated and measured S_{11} and peak gain of the proposed antenna.

structure. According to Fig. 4, the results of the BW and reflection coefficient intensity differ significantly from the expected values.

Similarly, a concentric circle was placed on the backside of the antenna structure to assess its impact on the BW and reflection coefficient depth, Fig. 5. As can be seen in the figure, none of the BW or reflection coefficient criteria were satisfied. Although BW may increase, return loss does not increase in the same manner, which proves the method's inefficiency.

In another simulation study, a concentric circle is located on both sides of the antenna (a total of two concentric circles), and parametric studies are conducted. Throughout this study, the radii of the concentric circles, R_1, vary equally at the same time. Considering the simulation results presented in Fig. 6, it can be concluded that this approach will not also produce estimated results.

In the next parametric simulation studies, the radii of the same concentric circles, R_1 and R_2, were swept with different amounts to evaluate the effectiveness of the method to increase the BW and improve the reflection coefficient in the frequency band, Fig. 7. Even so, this strategy will not provide the desired results for the BW and reflection coefficient of the proposed antenna, as seen in the figure. According to Fig. 7, some improvements have been made in the reflection coefficient and BW, but not to a sufficient degree.

As a final step, two concentric circles were located on the back side of the antenna, and their R_1 and R_2 radii were scanned separately. As presented in Fig. 8, both criteria were satisfied; BW covers 479–808 MHz (including 480–800 MHz) frequency spectrum, and reflection coefficient depth is more than −15 dB from 550 MHz to 750 MHz. The antenna was thus found to be compliant with the desired specifications. It met the reflection coefficient depth requirement of −15 dB from 550 MHz to 750 MHz, and the frequency spectrum of 480–800 MHz was also well covered. Results are obtained when R_1 and R_2 have 48.25 mm and 35.75 mm radii, respectively.

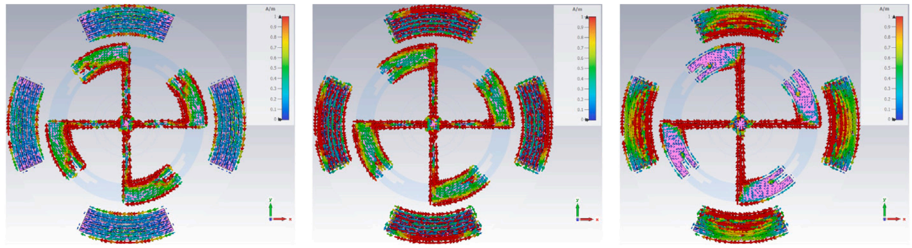

(a) @ 479 MHz. (b) @ 650 MHz. (c) @ 808 MHz.

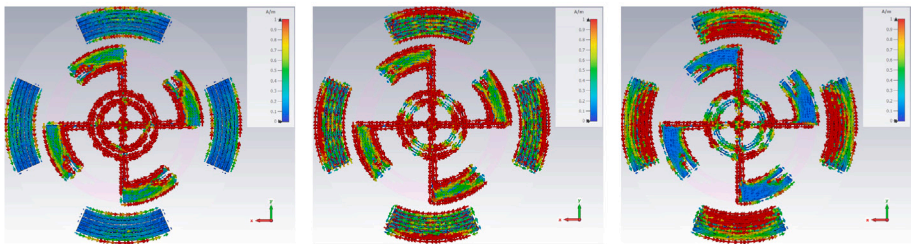

(d) @ 479 MHz. (e) @ 650 MHz. (f) @ 808 MHz.

Fig. 10. Simulated surface currents over the (a-c) top and (d-f) bottom layers of the proposed antenna.

3. Simulation studies and experimental results

In terms of the optimized values for the radius of the outer and inner concentric circles on the back-side of the antenna, the structure is made using an FR4 substrate. Network and spectrum analyzers are used to measure antenna return loss and gain in a free space and anechoic chamber, respectively. Based on the findings presented in Fig. 9, it appears that simulation and measurement results are in good agreement. There may be a small discrepancy between the simulated and measured reflection coefficients at the upper cutoff frequency of the BW as a result of the inhomogeneity of permittivity and loss tangent in the employed FR4 substrate, the measurement setup, and the tolerances in the company's antenna fabrication process. This discrepancy is further amplified by the effects of hardware restrictions on meshing and the consideration of hardware limitations in numerical simulations. However, the measured reflection coefficient is consistent with the simulated reflection coefficient across the BW. With a BW of 479–808 MHz, the proposed antenna covers the 550–750 MHz frequency band with less than −15 dB of reflection coefficient. With less than 0.215 dBi variations within the BW, the measured peak gain is consistent with the simulated peak gain, indicating gain stability for the proposed antenna structure. In fact, the peak gain within the BW is 0.90–1.35 dBi.

Based on the surface current density distribution over the parasitic elements and concentric circles, Fig. 10 illustrates their efficient function in enhancing gain and matching impedance across the BW.

At 650, 479, and 808 MHz frequencies, antenna radiation patterns in the E- and H-plane are measured for co-polarization and cross-polarization states in an anechoic chamber. With respect to the simulated and measured results, the E- and H-plane radiation patterns at 650 MHz have a Half Power Beam Width (HPBW) of 360° and 121.20°, respectively. It has an omnidirectional pattern in the E-plane, which makes it ideal for applications related to DTV. In Fig. 11, the E–11(a) and H-plane 11(b) radiation patterns at 650 MHz are shown in 2D normalized form as well as the 3D normalized form 11(c). Fig. 11(d)–11(i) present the same simulated and measured patterns at 479 and 808 MHz. Based on the illustrated information, the antenna exhibits a stable radiation pattern among its BW and maintains an omnidirectional E-field property. The co- and cross-pol patterns of the electric and magnetic fields at 650 MHz in cartesian coordinates are shown in Fig. 11(j) and 11(k) to clarify the variation in results. Simulated and measured results for the Cross-Polarization Discrimination (XPD) of the E- and H-field of the proposed antenna are presented in Fig. 11(l). For the E-field cross-pol, the XPD shows a considerable discrepancy due to the difference of 62.46 dB between the simulated and measured results.

Fig. 12 illustrates the simulated radiation efficiency, a crucial factor in assessing how well an antenna converts input power into radiated electromagnetic energy. Radiation efficiency ranges from 77.54 to 91.86 percent, depending on the antenna's BW.

Figs. 13(a) and 13(b) illustrate the front- and back-side of the constructed antenna, respectively. The measurement setup for measuring the return loss of the antenna structure is shown in Fig. 13(c).

Table 1 presents a comparison table demonstrating that the proposed antenna structure has broader HPBW at E-plane radiation patterns, making it an ideal candidate for use in DTV applications. Furthermore, it has a Fractional BW (FBW) of 50.77%, which is in excess of the requirements.

4. Conclusion

In this study, an omnidirectional wideband antenna with linear polarization is developed and analyzed for applications in the UHF spectrum, specifically for DTV broadcasting applications aboard ships where only linear and horizontal polarizations with omnidirectional patterns are needed due to the loss of signals received by linear and vertical polarizations. The antenna is designed to operate over the frequency range of 479 MHz to 808 MHz and has a measured reflection coefficient of less than −15 dB in the critical spectrum of 550 MHz to 750 MHz, with a peak gain range of 0.90 dBi to 1.35 dBi and variations of less than 0.215 dBi. Using the CPF excitation method in conjunction with an optimized planar structure containing parasitic elements and concentric circles, the structure meets the industrial compact size and lightweight specifications. The experimental validation aligns well with the simulated results, demonstrating reliable performance in both impedance bandwidth and gain stability. The antenna's omnidirectional radiation pattern, characterized by 360° and

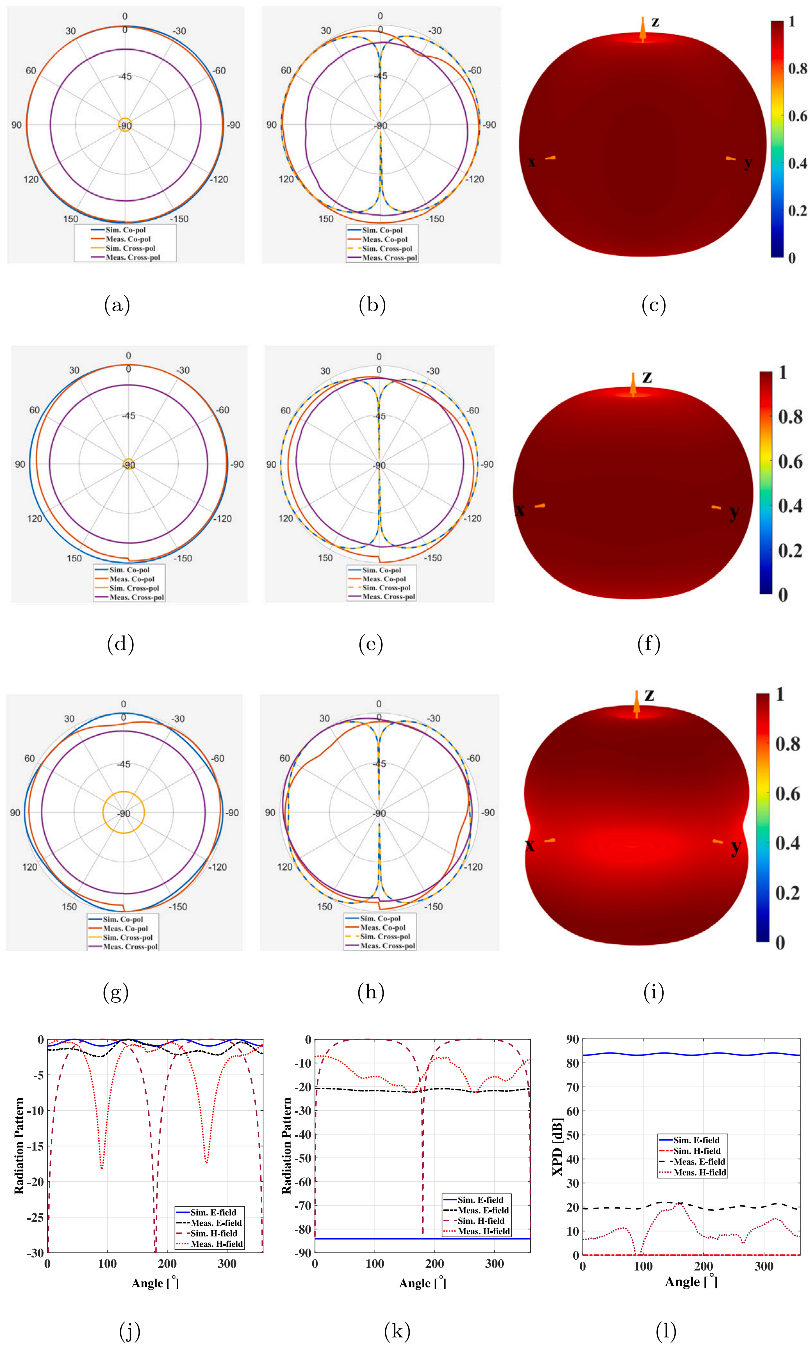

Fig. 11. Normalized simulated and measured radiation patterns of the proposed antenna are presented at 650 (a-c), 479 (d-f), and 808 MHz (g-i) for E-plane (a & d & g), H-plane (b & e & h), and 3D radiation pattern (c & f & i). Figures (j & k) illustrate the E- and H-field for the normalized simulated and measured radiation pattern at 650 MHz in Cartesian coordinates. Figure (l) depicts the simulated and measured radiation patterns' XPD for the E- and H-field at 650 MHz.

Table 1
Comparison with state-of-the-art UHF antennas spectrum.

Refs.	IBW [GHz] or FBW [%]	HPBW [°] or 3-dB ARBW [GHz]	Gain [dBiC]/[dBi]	Efficiency [%]	Polarization	Dimensions [λ^3]	Application
[2]	0.3–04/28.57 1.9–2.3/34.10	62 –	9.04–9.96 8.52–9.47	–	Circular	–	Satellite
[6]	0.404–0.871	70 –	−10–0.67	–	Linear	$0.19 \times 0.19 \times 0.008$	DTV Reception
[7]	0.458–0.782/62.34	–	1.1–2.95	–	Linear	$0.43 \times 0.4 \times 0.003$	DTV Application
[8]	0.36–0.50/32.5	27.2 –	6.7	–	Circular	–	UHF
[10]	1.6–2 3.25–4.95	–	−1.3–6.3	43.51 45.13	Linear	$0.53 \times 0.53 \times 0.005$	S-band & VHF-band
[11]	1.63–2.8/52.8	–	0.81–1.56	–	Linear	$0.55 \times 0.55 \times 0.057$	2G/3G/LTE
[12]	1.62–2.81/53.7	30 –	−0.9–1.3	–	Linear	$0.53 \times 0.53 \times 0.005$	2G/3G/LTE
[13]	1.72–4.46/37 2.45/4.1	–	1.3–2.7 4.3	71–95	Linear	$0.35 \times 0.14 \times 0.01$	UHF
[14]	1.925–1.955/1.54 2.36–2.48/4.95 3.502–3.53/0.73	–	1.2 1.6 −1.5	–	Circular	$0.32 \times 0.32 \times 0.14$	2G/3G/LTE
[15]	2–2.4/18	360	6.2–8.2	81–92 84–96	Linear	$1.08 \times 1.08 \times 0.01$	Beam Scanning
[16]	2.4–2.49/3.68 5.1–5.88/14.20	–	3.6–4.2 –	~90	Linear	$0.93 \times 0.5 \times 0.012$	2G/3G/LTE
This Work	0.479–0.809/50.77	E-plane: 360.00 H-plane: 121.20 –	0.90–1.35	77.54–91.86	Linear	$0.56 \times 0.56 \times 0.005$	DTV Reception

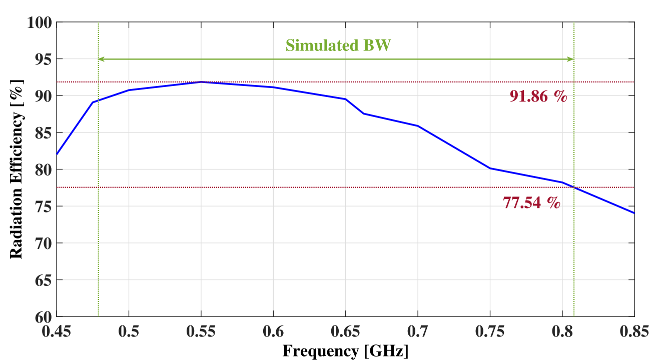

Fig. 12. Simulated radiation efficiency of the proposed antenna.

121.2° HPBW in the E- and H-plane, contributes to its suitability for DTV broadcasting by ensuring uniform signal coverage. Moreover, incorporating concentric circles improves bandwidth and return loss, satisfying design constraints while maintaining fabrication simplicity and cost-effectiveness.

CRediT authorship contribution statement

Shokooh Sadat Kooshki: Writing – original draft, Software, Data curation. **Fatemeh Dehghani:** Writing – review & editing, Validation, Software. **Keivan Kaboutari:** Writing – review & editing, Writing – original draft, Validation, Funding acquisition. **Javad Ghalibafan:** Writing – review & editing, Supervision, Data curation.

Declaration of competing interest

The authors declare the following financial interests/personal relationships which may be considered as potential competing interests: Keivan Kaboutari reports financial support was provided by Portuguese Foundation for Science and Technology. If there are other authors, they declare that they have no known competing financial interests or personal relationships that could have appeared to influence the work reported in this paper.

Acknowledgments

Keivan Kaboutari acknowledges co-financing by Fundação para a Ciência e a Tecnologia (Portuguese Foundation for Science and Technology) through the Carnegie Mellon Portugal Program under the fellowship PRT/BD/154201/2022.

(a) Front-side. (b) Back-side. (c) S-parameter measurement setup.

Fig. 13. Shots of the fabricated antenna and S-parameter measurement setup.

Data availability

No data was used for the research described in the article.

References

[1] Saunders S, Aragón-Zavala A. Antennas and propagation for wireless communication systems. Hoboken, NJ, USA: Wiley; 2007.

[2] Ren J, Shi J, Zhang Q, Zhang X, Liu Y. An UHF/S dual-band shared-aperture feed antenna for satellite application. IEEE Antennas Wirel Propag Lett 2024;23(7):2031–5. http://dx.doi.org/10.1109/LAWP.2024.3378011.

[3] Yu Y, Jolani F, Chen Z. A wideband omnidirectional horizontally polarized antenna for 4G LTE applications. IEEE Antennas Wirel Propag Lett 2013;12:686–9. http://dx.doi.org/10.1109/LAWP.2013.2264545.

[4] Kaboutari K, Maslovski S, Shokri M, Amiri Z, Ghobadi C, Nourinia J. Analytical models and equivalent networks of MED antennas. In: 2023 photonics & electromagnetics research symposium. 2023, p. 115–21. http://dx.doi.org/10.1109/PIERS59004.2023.10221341.

[5] Amiri Z, Kaboutari K, Ghobadi C, Nourinia J, Shokri M, Maslovski S. Modeling and design of improved-gain wideband magneto-electric dipole antenna for micro-BTS applications. Radio Sci 2024;59(11). http://dx.doi.org/10.1029/2024RS008037, e2024RS008037.

[6] Phongcharoenpanich C, Polkaew W, Luadang B, Akkaraekthalin P. A horizontally polarized omnidirectional antenna using stacked curve dipoles for DTV reception. Int J Antennas Propag 2015;2015(1):107148. http://dx.doi.org/10.1155/2015/107148.

[7] Teimouri M, Ghobadi C, Nourinia J, Kaboutari K, Shokri M, Virdee B. Broadband printed dipole antenna with integrated balun and tuning element for DTV application. AEU - Int J Electron Commun 2022;Vol. 148:pp. 154161. http://dx.doi.org/10.1016/j.aeue.2022.154161.

[8] Wang X, Liu M, Lu F. A spaceborne broadband circularly polarized conformal antenna for UHF band applications. Microw Opt Technol Lett 2024;66(3):e34115. http://dx.doi.org/10.1002/mop.34115.

[9] Ma Y, Li W, Han D, He Y, Li Q, Bai X, et al. Wireless wave attenuation in forests: An overview of models. Forests 2024;15(9):1587. http://dx.doi.org/10.3390/f15091587.

[10] Patil EC, Lokhande SD, Patil UA, Patil AU, Kumar J. Optically transparent dual-band antenna for UHF and S-band applications. Opt Mater 2024;147:114615. http://dx.doi.org/10.1016/j.optmat.2023.114615.

[11] Liu T, Yang H, He Y, Lu J. Cylindrical ring dielectric loaded horizontally polarized omnidirectional antenna for wideband radiation. AEU - Int J Electron Commun 2018;90:123–9. http://dx.doi.org/10.1016/j.aeue.2018.04.006.

[12] Cai Y-M, Li W, Hu W, Yin Y. A wideband compact horizontally polarized omnidirectional antenna for 2G/3G/LTE. Int J RF Microw Comput- Aided Eng 2018;28(5):e21256. http://dx.doi.org/10.1002/mmce.21256.

[13] Dang QH, Chen SJ, Nguyen-Trong N, Fumeaux C. Dual-band frequency-reconfigurable wearable antennas for UHF radio band applications. IEEE Trans Antennas and Propagation 2024;72(1):243–55. http://dx.doi.org/10.1109/TAP.2023.3320720.

[14] Cheng C, Zhang F, Yao Y, Zhang F. Triband omnidirectional circularly polarized dielectric resonator antenna with top-loaded alford loop. Int J Antennas Propag 2014;2014(1):797930. http://dx.doi.org/10.1155/2014/797930.

[15] Gao W, Chen SJ, Withayachumnankul W, Fumeaux C. Horizontally polarized 360° beam-steerable frequency-reconfigurable antenna. IEEE Trans Antennas and Propagation 2019;67(8):5231–42. http://dx.doi.org/10.1109/TAP.2019.2916612.

[16] Hu PF, Leung KW, Pan YM, Zheng SY. Electrically small, planar, horizontally polarized dual-band omnidirectional antenna and its application in a MIMO system. IEEE Trans Antennas and Propagation 2021;69(9):5345–55. http://dx.doi.org/10.1109/TAP.2021.3061096.